Muon Life Time

Report for the Advanced Lab Course

by

Yoshua Hempel

and

William Wenig

supervised by Dr. Marzieh Bahmani

Januar 2023, Berlin

Humboldt-Universität zu Berlin
Institut für Physik

Contents

Abstract

By utilizing an array of three NE102A plastic scintillators in conjunction with Hamamatsu H7360-02 photo multiplier combined in a logical circuit to process their NIM standard pulses with coincidence units, we measured the decay rates of Muons originating from cosmic ray particle showers. Through statistical evaluation of our measurements, in the form of a linear and non-linear fit, we were able to calculate the mean lifetime of the muon to be $\tau_\mu = 2.19(6)$ s.

Introduction

As it is mentioned in [Leo94] the scintillation detector is one of the most often and widely used particle detection devices in nuclear and particle physics. The applications for scintillators range from detecting particles, monitoring nuclear material all the way to the use in CT scanners for medical diagnostics. In this lab course we sought to measure the mean life time τ_μ of the Muon. For this we utilized an array of NE102A plastic scintillators so we could make use of their extremely low decay constant[1] of around $\tau = 2.4(1)$ ns (see [BM74] Table 2). In conjunction with them we used high-detection efficiency Hamamatsu H7360-02 photo multiplier with a spectral response in the range of 300 nm to 650 nm and a peak sensitivity wavelength of $\lambda = 420$ nm. As depicted in figure 7.5 in [Leo94] this matches with the light emission spectra of our scintillators.

1. Preparatory tasks

Our ensemble of scintillators and photo multipliers follows the structure depicted in figure 3 in [Bah22].

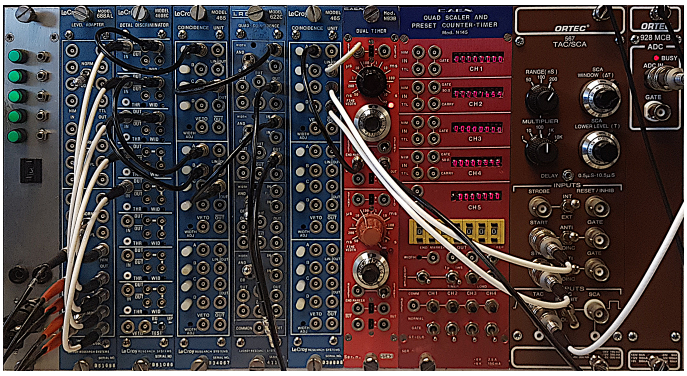

Figure 1: Setup for processing the signals of the photo multipliers. Shown is the configuration for the time calibration from figure 6 in [Bah22].

Each H7360-02 photo multiplier gave us a *positive* logic output with a pulse height of around 3 V. In order to convert the signals to a standard NIM signal, we fed these signals into the LeCroy 688AL level adapter, visible in figure 1 as the most left blue module. The TTL-to-NIM section of this level adapter accepts standard *negative* TTL logic signals, where

$$\text{logical "1"} \mathrel{\hat{=}} 0\,\text{V} \ldots 0.8\,\text{V} \quad \text{and} \quad \text{logical "0"} \mathrel{\hat{=}} > 2\,\text{V}.$$

In order to not get the complementary signal as an output[2], we flipped the switch on the level adapter to the COMPL position which sets it into the complementary operation. The TTL-to-NIM section of the level adapter yields a signal delay of around 6 ns.

To produce pulses of standard amplitude and duration we send the - now NIM signals - through a LeCroy 4608C octal discriminator. Its output signals are logic pulses in response to its input exceeding a given threshold. The delay of this module is smaller than 18 ns.

1.1. Coincidence unit signal delay

To build the logic circuit depicted in figure 7 in [Bah22] we used three coincidence units of two kinds. Two LeCroy 465 which support AND-logic and one LRS 622C capable of OR- and AND-logic. With the now prepared signals we proceeded to find out the signal delay of the one subunit of each type of coincidence unit.

To do this we used the output of the photo multiplier PM2 which we connected both to one channel of the Tektronix TDS3032B oscilloscope and to one of the two types of coincidence units we used. We then connected the output of this coincidence unit to the second channel of the oscilloscope. This way we were able to see the same signal on the different channels with a delay characteristic of the coincidence unit we tested, as well as the cables connecting everything. We used the same cables for both subunits of the coincidence units.

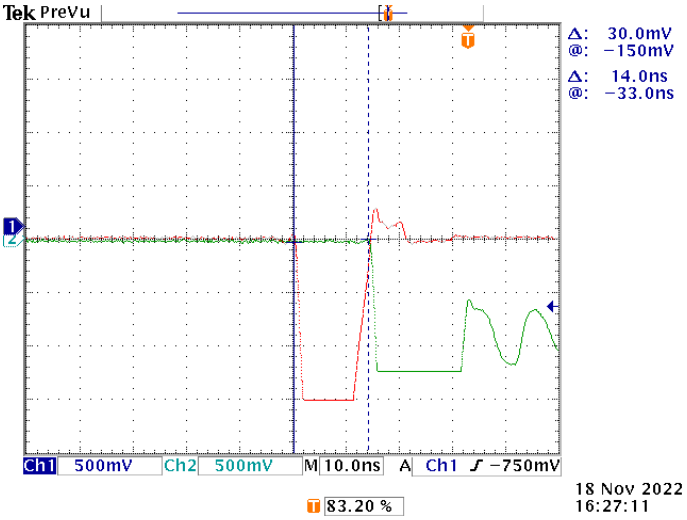

Figure 2: Image of the measurement for the signal delay of a subunit of the LeCroy 465 coincidence unit. The red line depicts the signal we got from the photo multiplier PM2. The green line depicts the signal we got from PM2 whilst running its signal through the coincidence unit.

The first subunit we analyzed was one of the LeCroy 465 modules. We measured its signal delay to be[3]

$$\delta_{\text{CU1}} = (14.0 \pm 0.4)\ \text{ns}.$$

The measurement is depicted in figure 2 with the two cursors that we used to determine the time interval between the two signals.

The second subunit we analyzed was one of the four of the LRS 622C. We measured the signal delay analogously in figure 3 which turned out to be

[1] Where we assumed a Gaussian Error of one last figure quoted after Section 2.8.1 in [HH10].

[2] We fed *positive* logic into the adapter that then gives out *negative* logic output.

[3] The investigation of the associated error is depicted in section 2

$$\delta_{CU2} = (12.6 \pm 0.4)\ \text{ns}.$$

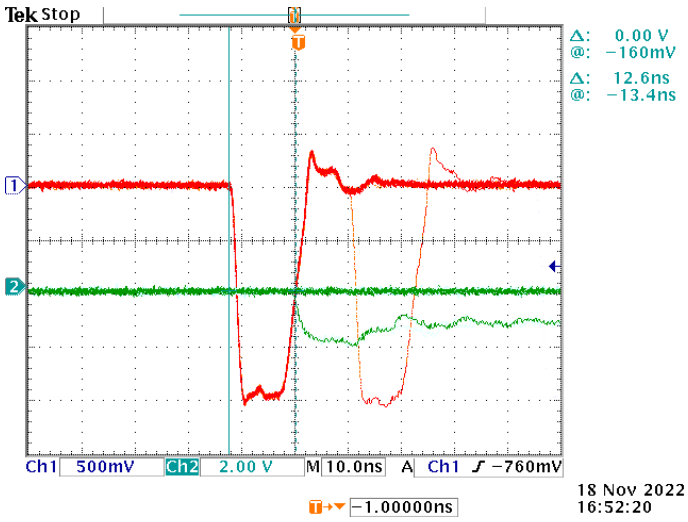

Figure 3: Image of the measurement for the signal delay of a subunit of the LRS 622C coincidence unit. The red line depicts the signal we got from the photo multiplier PM2. The green line depicts the signal we got from PM2 whilst running its signal through the coincidence unit.

Unfortunately there are no reference values given by the manufacturer to which we can compare our obtained delay times. δ_{CU1} and δ_{CU2} are of the order of magnitude of the signal delay time of the discriminator. That they do not agree with each other is nothing that surprises us because the two kinds of coincidence units are built for different purposes.

The sum of all mentioned signal delay times (which do not include the influence of cables yet) is around 3% of the expected value of the Muon's mean lifetime. As this will only influence the final measurement perceivably if the other sources of uncertainty are within that range of confidence, we will go into further detail of this influence in the following sections.

When looking at figure 2 and 3, it becomes clear however, that the delay times δ_{CU1} and δ_{CU2} are not negligible compared to the width of the pulses. Because of this, two originally coincidental signals could temporally drift apart when not sent through the same sequence of modules and cables.

1.2. Event rates

In section 3 of [Bah22] it is mentioned that the scintillators SC2 and SC3 are equipped with two photo multipliers each to increase the noise suppression. In order to observe this, we counted event rates of different logically connected configuration. We used the CAEN N145 quad scaler and preset counter-timer depicted in figure 1. In one of the four upper sections of the quad scaler we gave the output of the current configuration as NIM input and used it in GATE mode. This means the counter would only be incremented by input pulses if the GATE input is true. As the GATE input we used the output in section 5 of the quad scaler that delivers true as long as the pre-set counter contents are different from zero. We set the counter to 1 s. Pushing the LOAD button starts the process and increments the counter in one of the used upper four sections. The event rates we obtained and their respective errors are depicted in table 1. Because the counted events will follow a Poisson distribution, we calculated the uncertainties as shown in [HH10] section 3.4.

Table 1: Event rates measured with different configurations, including the standard deviation

Configuration	Mean Event Rate $\langle x \rangle$ [s^{-1}]
PM1	1390(40)
PM2	770(27)
PM3	1130(30)
PM4	1160(30)
PM5	890(29)
(PM4∧PM2)∨(PM3∧PM5)	303(17)
SC1 ∧ SC2	31(6)
SC1 ∧ SC2 ∧ SC3	12.2(3)
SC1 ∧ SC2 ∧¬ SC3	25(5)
SC2 ∧ SC3	19(4)
SC2 ∨ SC3	307(17)
SC1 ∧¬ SC1 ∧¬ SC3	1300(40)
¬ SC1 ∧ SC2 ∧¬ SC3	129(11)
¬ SC1 ∧¬ SC2 ∧ SC3	161(13)
SC2	141(12)
SC3	169(13)

The first observation that can be made is that by combining the photo multipliers PM2 and PM4 as well as PM3 and PM5 with a logical AND, reduced the amount of measured events by almost 90%, showing that it is indeed very efficient at reducing noise. Beyond that the relationship between the event rates of different combinations of scintillators appears to be sensible. As one would expect in the case of random events such as noise, there is a hierarchy of event rates where an SCi ∨ SCj combination has a higher rate than a SCi ∧ ¬ SCj one, which has a higher rate than a SCi ∧ SCj combination with $i \neq j$.

2. Time Calibration

The actual measurement of the mean life time of the Muon involves the usage of the Ortec 567 time to amplitude converter (TAC), that you can make out as the first brown NIM module in figure 1.

2.1. Workings of the equipment

The TAC measures the time interval τ between pulses to its START and STOP inputs and generates an output pulse of a height U such that U is between 0 V and 10 V and $U \propto \tau$. It accepts negative and positive NIM logic signals on its START and STOP inputs.

When the TAC registers a pulse from START it disables further signals from that input and waits for an input from STOP. We set the TAC to wait 20 µs upon receiving the START input pulse via nobs on the front panel. In this time interval the TAC can receive a pulse from STOP after which the time conversion is terminated.

The TAC output is then fed into the ADC IN on the Ortec 928 MCB module in figure 1. This converts the analog signal from the TAC into a digital one which we then save via a USB-2.0 interface. The Ortec 928 MCB converts the pulse height U into a channel number $n \in \mathbb{N}$ with a maximum resolution of 16384 channels.

The task was to find the constant ω that translates our channel numbers n into our originally measured time intervals τ. For this we constitute a simple linear function

$$\tau(n) = \omega \cdot n + \tau_0. \tag{2.1}$$

The only thing that had to be done from then on, was to create pairs of pulses separated by a time interval τ that we could modify at the interface on one of our NIM modules.

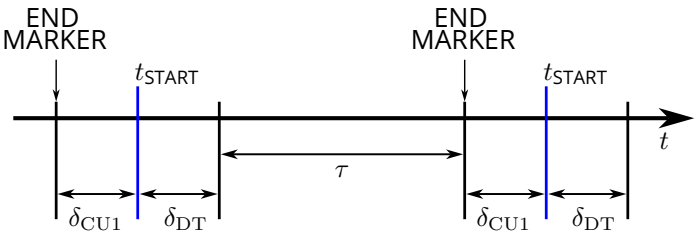

Figure 4: Time intervals of the self-running rate generator where the travel time of the cables is neglected. δ_{CU1} is the signal delay time of the LeCroy 465 coincidence subunit. δ_{DT} is the input-output delay time of the dual timer. τ represents the time set on the dual timer from equation (2.1). Assuming the LIN. OUT and OUT delay times have a negligible difference t_{START} is the moment the TAC receives the START and STOP pulses.

We used the CAEN N93B dual timer in figure 1 for this purpose in combination with one of the 465 coincidence units next to it. We constructed a self running rate generator by feeding the END MARKER output into the 465 coincidence unit. We then fed the linear output[1] into the START of the dual timer and used the other two regular outputs as inputs for START and STOP on the TAC.

In figure 4 we depicted the timing of the generator assuming that the delay time of the cables are negligible and that the delays of the LIN. OUT and OUT have a negligible difference. By this, the real time intervals that are measured by the TAC would be

$$\tau' = \delta_{CU1} + \tau + \delta_{DT}. \tag{2.2}$$

[1] The linear output (LIN. OUT) does not undergo an additional pulse forming stage compared to the regular output (OUT). In this the pulse width can be adjusted by the potentiometer on the rear panel of the coincidence unit.

We decided to neglect this influence because for the time intervals τ we conducted

$$1 + \eta = 1 - \frac{\delta_{CU1} + \delta_{DT}}{\tau'} = \frac{\tau}{\tau'} \approx 96.5\% \ldots 99.8\%.$$

We also conclude from this that it is a good idea to measure bigger time intervals where $\eta \ll 0$ is closer to being satisfied.

2.2. Fitting to the linear model

For measuring the time interval τ' between the pules of the rate generator we fed another output into the oscilloscope.

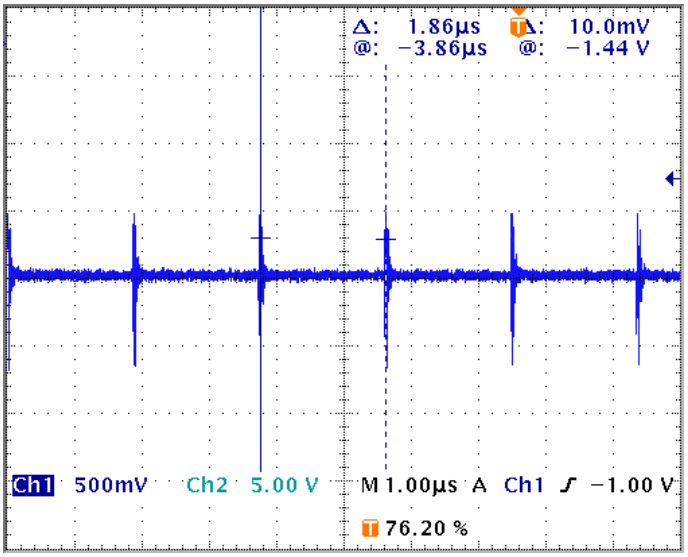

Figure 5: Screenshot from the oscilloscope for the measurement of the time delay τ'. The cursors were set using the magnification tool to ensure precision when selecting.

Figure 5 illustrates the measurement similar to those in the previous section. By performing this measurement we obtained the data depicted in table 2 and figure 6.

Table 2: Obtained i-th measurement for translating the channel numbers n into the corresponding delay times τ' including each channel width Δn.

i	τ' [µs]	n	Δn	i	τ' [µs]	n	Δn
1	0.78(12)	157(4)	1	12	3.80(12)	788(4)	1
2	0.94(12)	193(4)	2	13	4.08(12)	844(4)	1
3	1.28(12)	261(4)	2	14	4.34(12)	894(4)	1
4	1.58(12)	326(4)	2	15	4.60(12)	948(4)	2
5	1.86(12)	384(4)	2	16	5.9(5)	1223(4)	1
6	2.16(12)	445(4)	2	17	8.2(5)	1729(4)	2
7	2.44(12)	504(4)	1	18	10.5(5)	2189(4)	2
8	2.72(12)	564(4)	1	19	12.6(5)	2880(4)	4
9	3.02(12)	618(4)	1	20	13.8(5)	3343(4)	5
10	3.28(12)	675(4)	2	21	16.1(5)	3726(4)	6
11	3.54(12)	733(4)	1				

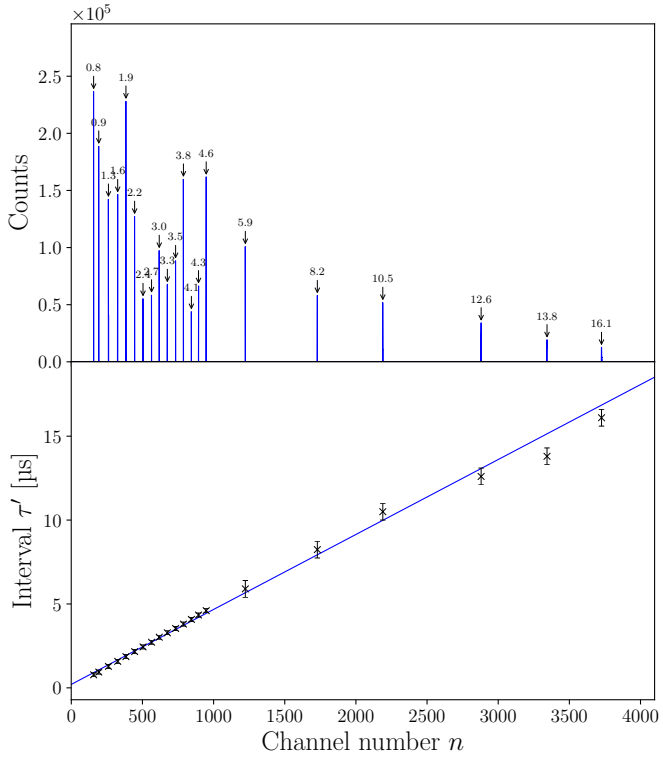

Figure 6: Representations of the data from table 2. The upper histogram illustrates the data from the 928 MCB. It shows the number of counts of each channel number. The superscripts above the bins depict the measured τ' that corresponds to the channel number of that bin. The lower plot shows τ' against the channel number n with a best fit line. For n, error bars are smaller than the symbol size.

For the uncertainty in τ' we only found out that the TDS3032B in a time measurement ≥ 1 ms yields a time base accuracy of 20 ppm. For a time base of 1 µs this corresponds to an accuracy of around 80 ps. We were sure that the process of selecting the peak correctly with the cursors in figure 5 contributes an uncertainty that is at least five orders of magnitude bigger. When conducting the measurement one has to set the two cursors on the positions of the two peaks. For this we incorporated that we could miss the peaks by three pixels. This results in the heteroscedastic data quoted in table 2 where we used time bases of 1 µs and 4 µs.

Table 3: Best fit parameters and statistics of the fit obtained in the lower plot in figure 6. $\rho_{\omega\tau_0}$ is the correlation coefficient of ω and τ_0 and $\mathcal{D}$ the *Durbin-Watson* statistic.

Parameters	
ω [µs]	τ_0 [µs]
$4.47(8)\cdot10^{-3}$	0.21(5)

Statistics			
χ^2	χ^2_ν	$\rho_{\omega\tau_0}$	$\mathcal{D}$
20.68	1.09	-0.83	0.48

For the uncertainty in the channel numbers n we used 0.1% of the highest channel for which we observed counts, as we found no further reading on the precision of the 928 MCB.

In the lower portion of figure 6 we have illustrated the data in combination with its best fit to the model from equation (2.1). The corresponding parameters to this fit are presented in table 3.

2.3. Quality of the fit

As the error bars in figure 6 represent a 68% confidence limit, roughly two thirds of the data should be consistent[1] with the best fit line. As 86% of our observed data points lie withing the model from equation (2.1) we can say that this model makes a great candidate for further investigation.

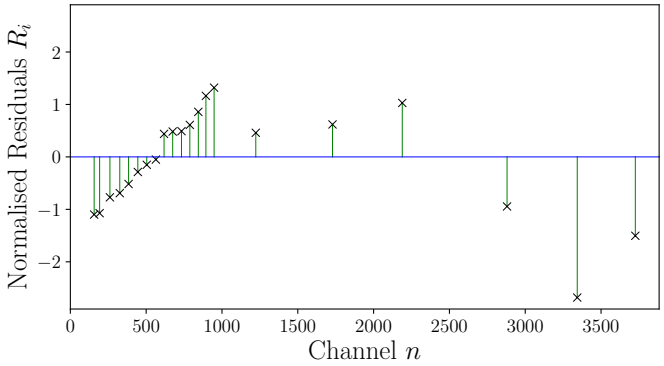

Figure 7: Plot of the normalized residuals R_i for the fit in figure 6. The green lines are a guide to the eye.

Because of our heteroscedastic data, we will start the investigation by looking at the *normalized* residuals in figure 7. In our case they are defined as

$$R_i = \frac{\tau'_i - \tau(n_i)}{u_{\tau'}}.$$

Consistent with the statement before we can clearly see that 71.4% of them satisfy $|R_i| \leq 1$ and 95% satisfy $|R_i| \leq 2$, which is expected[2] for a good fit. However as we mentioned before, we used two different time bases on the oscilloscope. In figure 7 we can see that for the time intervals measured with the 1 µs time base, the residuals do not seem to be scattered. They have a linear trend, which gives rise to the assumption that there is a systematic discrepancy in the model. This assumption is further strengthened by visualizing the structure in the residuals with a lag plot.

In figure 8 we plotted the i-th normalized residual against the (i–1)-th. This reveals the positive trend of the residuals. As any non-random pattern in the lag plot is an indicator of autocorrelations in the residuals[3] this suggests that the model is incomplete for the data we have observed. This is the case although we, again, see that in figure 8, 90% of the residuals are contained withing $\pm 2\sigma$.

[1] The best fit line intersects with the error bars.
[2] See [HH10] section 6.3.2.
[3] See [HH10] section 6.7

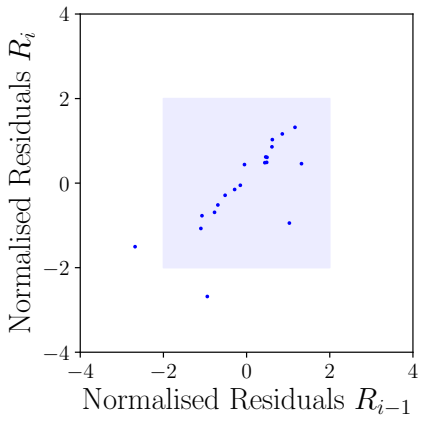

Figure 8: A lag plot for the fit done in figure 6. The blue box indicates the region that is contained withing $\pm 2\sigma$ of the normalized residuals.

The *Durbin-Watson* statistic $\mathcal{D}$ depicted in table 3 reflects this discussion as well. It is defined as mentioned in [HH10] section 6.7 as

$$\mathcal{D} = \frac{\sum_{i=2}^{N} \left[R_i - R_{i-1}\right]^2}{\sum_{i=1}^{N} \left[R_i\right]^2} \tag{2.3}$$

and has a range of $0 < \mathcal{D} < 4$. For our obtained value in table 3 it approaches the limiting case of 0 which suggests systematically correlated residuals.

Furthermore we look at the minimal achieved goodness-of-fit parameter χ^2. For a reasonable fit $\chi^2 \approx \nu$ where ν is the amount of degrees of freedom or $\chi^2_\nu \approx 1$ for the *reduced* χ^2. For our two-parameter fit we see from table 3 that $\nu = 19$. As we expect a χ^2 withing two standard deviations of the mean[1] the null hypothesis shall not be rejected[2] if our obtained minimal value for χ^2 satisfies the following criterion

$$\nu - 2\sqrt{2\nu} \leq \chi^2 \leq \nu + 2\sqrt{2\nu} \tag{2.4}$$

$$\Rightarrow \qquad 6.67 \leq \chi^2 \leq 31.32 \tag{2.5}$$

As the value quoted in table 3 fulfills this criterion, we do not reject the hypothesis that our data is well modeled by the model (2.1). As the *reduced* χ^2, χ^2_ν, approaches 1 we say that the linear model is is a reasonable way of describing the translation from channel numbers n into the time intervals τ'. But because of the systematic discrepancies that were revealed in figures 7 and 8 we think that collecting more data is important to check for reproducibility and to find out where this behavior originates.

3. Measurement of the Muon Lifetime

With the TAC calibration complete, we were now able to begin the measurement of the mean life time of the Muon. For this purpose, we set up the circuit illustrated in figure 7 of [Bah22]. With it we want to measure the time intervals between (a) the arrival of the Muon at SC1 and SC2 and (b) its decay in the Aluminum between SC2 and SC3. Using the N93B dual timer allowed us to limit the number of measured events to those that happened within a set range of time. At fist we initiated a 30-minute measurement in which we didn't restrict the number of measured events with the dual timer.

3.1. Unrestricted measurement

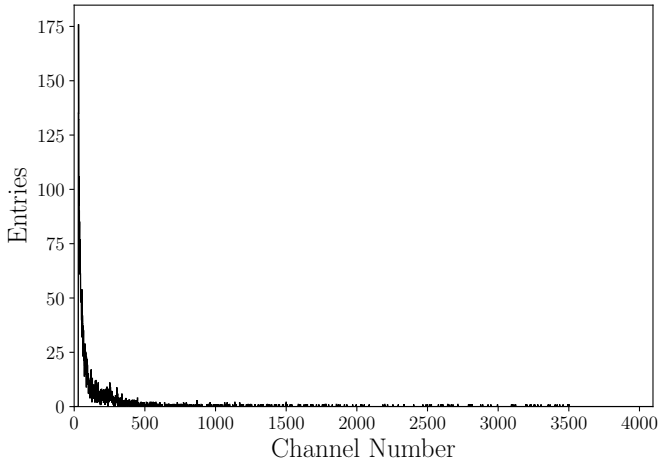

Figure 9: Data from the 928 MCB without setting up a delay with the N93B dual timer.

Figure 9 demonstrates the necessity of setting up a delay time as a minimum length for measured events, as otherwise the beginning of the spectrum dominates with a large peak, which would makes a fit difficult[3]. One cause of this may be Muons which retained a high enough energy to pass through the detector with low chance of decay but slow enough not to trigger a coincidence in SC1, SC2 and SC3.

3.2. Restricted measurement

Because of this we set up a delay time of 3 µs, as well as an upper bound of 17 µs. After that, only events with a duration between 3 and 20 µs were accepted. In order to reduce the influence of noise on the spectrum we rebinned the channels of the spectrum up to a point, where the overall shape was preserved. We chose a binwidth of 40, which suppressed a lot of noise without changing the shape of the distribution too much. In figure 10 the data of the final 24-hour measurement is depicted.

As discussed in section 2.1.1 of [Bah22], the decay of muons inside the Aluminum block is described by the following function, where N_{μ^+} is the total count of positively charged muons, $f = N_{\mu^-} N_{\mu^+}^{-1}$ is the ratio of negatively charged muons to positively charged muons, Q is the huff factor of the Aluminum and Λ_C is the capture rate of negatively

[1] Of the parent distribution of the χ^2 statistic.
[2] See [HH10] section 8.4.
[3] Meant is the difficulty of performing a numerically stable fit.

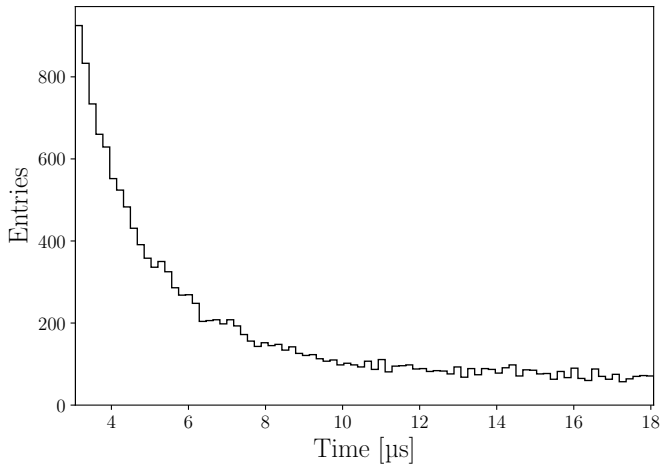

Figure 10: Data from the 928 MCB of the 24-hour measurement with setting up a delay with the N93B dual timer and rebinning with a bin width of 40.

charged muons in the Aluminum.

$$N_\mu(t) = N_{\mu^+}\left(e^{-\frac{t}{\tau_\mu}} + f^{-1}e^{-t\left(\frac{Q}{\tau_\mu}+\Lambda_C\right)}\right) \tag{3.1}$$

Now we did not measure the amount of muons directly, instead we counted how many muons decayed within certain time intervals (t_1, t_2), the width of which is given by the binning. By this model the expectation for the amount of muons counted in the k-th bin is

$$N_{\mu k} = N(t_k) - N(t_{k+1}). \tag{3.2}$$

In first order approximation this is equal to

$$N_{\mu k} = -\frac{\mathrm{d}N_\mu}{\mathrm{d}t}(t_k)(t_{k+1} - t_k) = -\frac{\mathrm{d}N_\mu}{\mathrm{d}t}(t_k)\Delta t \tag{3.3}$$

$$= N_{\mu^+}\left(\frac{1}{\tau_\mu}e^{-\frac{t}{\tau_\mu}} + f^{-1}\left(\frac{Q}{\tau_\mu}+\Lambda_C\right)e^{-t\left(\frac{Q}{\tau_\mu}+\Lambda_C\right)}\right)\Delta t, \tag{3.4}$$

where Δt is the width of the bins. We must also consider that background events will influence our measurements, such as thermal sources of radiation in our detector elements. This noise leads to an additional constant probability of random uncorrelated signals, which could be read as a muon having entered the detector if a signal in SC1 and SC2 occurs simultaneously or more likely, as a Muon having decayed if SC2 or SC3 send out a signal after a Muon has entered the Aluminum block. We want to account for the latter type of background events by adding another term to our fit function. If we look at the event rates of the scintillators SC2 and SC3 in table 1, we see that they are in the range of about 150 events per second. Since in our setup, a background event setting off SC2 or SC3 after a Muon has entered the detector is equivalent to measuring a Muon decay, we can modify our count of Muons that haven't decayed until time t. We introduce the function $N(t)$ which represents the amount of muons that have neither decayed nor had a background event happen in SC2 or SC3 before decaying. With the constant background event rate λ this can be written as

$$N(t) = N_\mu(t) - N_{\mu^+}(1 + f^{-1})\lambda t. \tag{3.5}$$

Through the same steps as above, this leads to an expected count in bin k of

$$N_k = \left(-\frac{\mathrm{d}N_\mu}{\mathrm{d}t}(t_k) + N_{\mu^+}(1 + f^{-1})\lambda\right)\Delta t \tag{3.6}$$

$$:= F(t_k) \tag{3.7}$$

Since the parameter N_{μ^+} only appears in a product with Δt we will combine them to a fit parameter $\tilde{N} = N_{\mu^+}\Delta t$. The fit itself will be done through the method of minimizing the χ^2 parameter. Because the individual bins are from a parent Poisson distribution, the proper form of χ^2 is[1]

$$\chi^2 = \sum_k \frac{(F(t_k) - N_k^{\text{measured}})^2}{F(t_k)}. \tag{3.8}$$

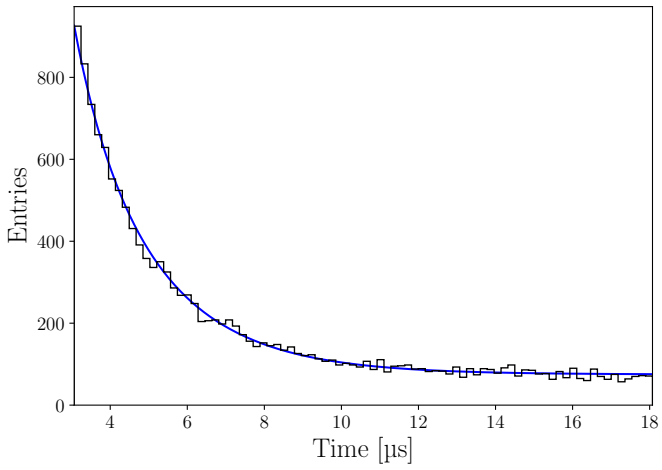

Figure 11: Data from the 928 MCB of the 24-hour measurement with setting up a delay with the N93B dual timer. The blue line illustrates the best fit $F(t)$ to the muon decay spectrum with a minimal $\chi^2 = 72.46$.

Table 4: Obtained fit parameters for $F(t)$ from figure 11.

Parameter	Value with standard errors
$\tilde{N}$ [10^3 µs]	6.12(17)
λ [ms^{-1}]	6.84(18)
τ_μ [µs]	2.19(5)

With 84 channels and three fit parameters, we calculated the reduced χ^2 with $\nu = 81$ degrees of freedom.

$$\chi^2_\nu \approx 0.89 \tag{3.9}$$

[1] See [HH10] section 6.1.1.

This value for the reduced χ^2 is quite close to 1 which could indicate that the chosen expected parent distribution coincides well with the data. With the parameter ω from the calibration, which represents the width of the channels before rebinning and the rebinned binwidth of 40, the value of Δt can be calculated. This can then be used to acquire an estimate for the amount of positive muons which have entered the detector during the 24 hours of measurement and consequently the total amount of muons N_μ^{total}. This number only represents the number of muons which were slowed down enough, to not trigger a coincidence in SC1, SC2 and SC3.

$$\begin{aligned} \Delta t = 40 \cdot \omega &= 0.179(3) \\ N_{\mu^+} = \tilde{N} \cdot \Delta t^{-1} &= 3.43(11)\ 10^4 \\ N_\mu^{\text{total}} = N_{\mu^+} \cdot (1 + f^{-1}) &= 6.12(20)\ 10^4 \end{aligned}$$

In order to gauge the influence of the parameters' f and Λ_C uncertainties, which are included in the fit function on the result for $\tau_m u$, we tested how the parameter changes when changing them by their errors. It must be said that

Table 5: Highest difference in τ_μ when modifying a parameter by their uncertainty

	$\Delta f = \pm 0.003$	$\Delta \Lambda_C = \pm 13\ \text{ms}^{-1}$
$\Delta \tau_\mu$	± 0.01 µs	± 0.01 µs

we would expect the true deviation of the parameter f to be larger, as the capture of negative muons before entering the Aluminum block should increase the ratio of positive to negative muons, since they didn't just travel through air but also the block of lead as well as the building surrounding the setup. Combining the deviations we get when varying the parameters of f and Λ_C, we get a systematic error of $\sigma_{\text{sys}} = 0.02$. Another source of systematic error would be the delay times of the electrical devices and cables, which is in the range of 10 ns, however what is measured is the time difference between a start and a stop signal which are both delayed ideally by the same amount of time as they both run through all of the coincidence units. As such only the variance in delay times should influence the measurement, which is most likely negligible as the delay times themselves are only in the magnitude of the last significant digit of the statistical uncertainty.

As such our final measurement for the muon lifetime is

$$\tau_\mu = 2.19(6). \tag{3.10}$$

This value coincides very well with that from the literature of $\tau_\mu = 2.19703(4)$ µs, although our uncertainty might indicate that this was coincidental. Still our results, especially pertaining to the quality of the fit, show the efficiency of scintillators in combination with the filtering out of unwanted events with the help of coincidence units for measuring the decay rate of muons. By doing further work to eliminate noise and stabilize measurement conditions, as well as increasing the sample size, it could probably lead to even more precise measurements of the lifetime.

References

[Bah22] M Bahmani. *Measurement of the muon lifetime. Experimental instructions for the advanced internship*. Humboldt-Universität zu Berlin. AG Experimental Elementary Particle Physics, 2022.

[BM74] B. Bengston and M. Moszyński. "Energy-Transfer And Light-Collection Characteristics For Different Types Of Plastic Scintillators". In: *Nuclear Instruments And Methods* 117.1 (1974), pp. 227–232. DOI: https://doi.org/10.1016/0029-554X(74)90401-7.

[HH10] I. Hughes and T. Hase. *Measurements and their Uncertainties: A Practical Guide to Modern Error Analysis*. Oxford University Press Inc., 2010. ISBN: 978-0-19-956632-7.

[Leo94] R. William Leo. *Techniques for Nuclear and Particle Physics Experiments. A How-to Approach*. 1994. ISBN: 9783540572800.